ACS APPLIED MATERIALS & INTERFACES

Research Article

www.acsami.org

Hybrid Cu_2O Diode with Orientation-Controlled C_{60} Polycrystal

Masanobu Izaki,*[,†,‡] Takamasa Saito,[†] Tatsuya Ohata,[†] Kazufumi Murata,[†] Binti Mohamad Fariza,[†] Junji Sasano,[†] Tsutomu Shinagawa,[§] and Seiji Watase[§]

[†]Graduate School of Engineering, Toyohashi University of Technology, Toyohashi, Aichi 441-8580, Japan

[‡]JST, CREST, 5, Sanban-cho, Chiyoda-ku, Tokyo 102-0075, Japan

[§]Osaka Municipal Technical Research Institute, Morinomiya, Joto-ku, Osaka 536-8553, Japan

ABSTRACT: We report on a hybrid diode composed of a 2.1 eV bandgap p-cupric oxide (Cu_2O) semiconductor and fullerene (C_{60}) layer with a face-centered cubic configuration. The hybrid diode has been constructed by electrodeposition of the 500 nm thick Cu_2O layer in a basic aqueous solution containing a copper acetate hydrate and lactic acid followed by a vacuum evaporation of the 50 nm thick C_{60} layer at the evaporation rate from 0.25 to 1.0 Å/s. The C_{60} layers prepared by the evaporation possessed a face-centered cubic configuration with the lattice constant of 14.19 A, and the preferred orientation changed from random to (111) plane with decrease in the C_{60} evaporation rate from 1.0 to 0.25 Å/s. The hybrid p-Cu_2O/C_{60} diode showed a rectification feature regardless of the C_{60} evaporation rate, and both the rectification ratio and forward current density improved with decrease in the C_{60} evaporation rate. The excellent rectification with the ideality factor of approximately 1 was obtained for the 500 nm thick (111)-Cu_2O/50 nm thick (111)-fcc-C_{60}/bathocuproine (BCP) diode at the C_{60} evaporation rate of 0.25 Å /s. The hybrid Cu_2O/C_{60} diode prepared by stacking the C_{60} layer at the evaporation rate of 0.25 Å/s revealed the photovoltaic performance of 8.7×10^{-6}% in conversion efficiency under AM1.5 illumination, and the conversion efficiency changed depending on the C_{60} evaporation rate.

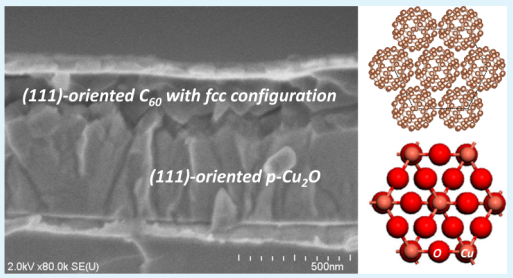

KEYWORDS: *copper oxide, fullerene, hybrid, diode, rectification, ideality factor*

1. INTRODUCTION

Hybrid diodes composed of inorganic and organic semiconductors have attracted increasing attention in electronic applications, especially the photovoltaic device.[1] There have been many reports on hybrid ZnO diodes with organic semiconductors including phenyl C_{61} butyric acid(PCBA)[2] and poly[2-methoxy-5-(3′,7′-dimethyloctyloxy)-1.4-phenylenevinylene] (MDMO-PPV).[3] The mechanism for generating photocurrent in organic photovoltaic devices is believed to be due to the creation of bond excitons that is pairs of electron and hole by absorbing light in the active organic semiconductor of the devices. The generation of carriers was resulted from the dissociation of excitons by high internal electric field generated at the interface to another organic semiconductor and to inorganic semiconductor layer such as a transparent conductive window in organic photovoltaic devices.[4,5] The ZnO layer introduced into the hybrid diode plays a role in accelerating the dissociation of the excitons and reducing any recombination loss, and the ZnO layer does not act as a light-absorbing layer due to its band gap energy of 3.3 eV.

Cu_2O is a p-type semiconductor with the band gap energy of 2.1 eV and high absorption coefficient of the order of 1×10^4 cm^{-1} and has attracted increasing attention as a light-absorbing layer in photovoltaic devices.[6,7] The high-quality Cu_2O layer, which emits visible light because of the recombination of the phonon-assisted exciton at room temperature, has been prepared by heteroepitaxial electrodeposition on a (111)-Au/(100)-Si wafer substrate.[8] The fullernene (C_{60}) is an indispensable component as the acceptor in organic photovoltaic devices, and the C_{60} solid with a face-centered cubic configuration is a semiconductor with the direct energy gap of 1.5 eV.[9,10] The (111)-oriented C_{60} layer with the face-centered cubic configuration could be obtained on Si[11] and mica substrates[12] by heteroepitaxial growth using gas phase deposition techniques, and the preferred orientation changed depending on the preparation conditions such as the deposition rate and substrate temperature. The hybrid Cu_2O/C_{60} diode is a potential candidate of the fundamental configuration for hybrid electronic devices including photovoltaic devices, because both layers act as the light-absorbing layer, and that the Cu_2O layer plays a role in accelerating the dissociation of excitons generated in the C_{60} layer due to the dielectric constant. The Cu_2O/C_{60} hybrid diode has been prepared by electrodeposition of the Cu_2O layer followed by vacuum evaporation of C_{60} and showed the conversion efficiency of 4.2×10^{-3}%.[13]

Here, we construct the hybrid p-Cu_2O/C_{60}/Bathocuproine-(BCP) hybrid diode on an Au(111)/(100)Si wafer substrate by electrodeposition of the Cu_2O layer followed by vacuum evaporation of the C_{60} layer at the evaporation rate from 0.25 to

Received: April 8, 2012
Accepted: June 18, 2012
Published: June 18, 2012

   dx.doi.org/10.1021/am3006093 | ACS Appl. Mater. Interfaces 2012, 4, 3558−3565

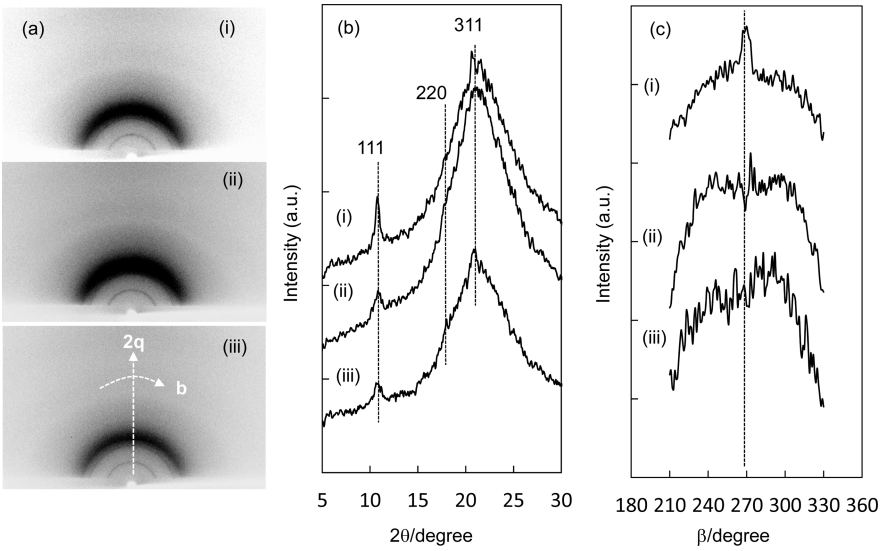

Figure 1. (a) X-ray diffraction patterns,(b) 2θ intensity, and (c) β-intensity curves for C_{60} layers prepared at evaporation rate of (i) 0.25, (ii) 0.50, and (iii) 1.0 Å/s.

1.0 Å/s, and the structural and electrical characterizations were carried out. The C_{60} layers possessed a face-centered cubic configuration, and the preferred orientation changed from random to (111) plane with decrease in the evaporation rate from 1.0 to 0.25 Å/s. BCP is a material with the wide bandgap energy of 3.5 eV,[14] and the insertion of the thin BCP layer between the C_{60} and metallic electrode induced the increase in the power conversion efficiency, especially the increase in open-circuit voltage (Voc).[15] The BCP layer played roles to block holes in addition to confining excitons and to prevent the creation of donor-state in the C_{60} layer by the Al in an indium tin oxide (ITO)/phthalocyanine/C_{60}/BCP/Al photovoltaic device. The rectification characteristic of the Cu_2O/C_{60}/BCP diode changed depending on the C_{60} evaporation rate, and the hybrid (111)-Cu_2O/(111)-C_{60}/BCP diode revealed an excellent rectification feature with the ideality factor of about 1. The hybrid Cu_2O/C_{60}/BCP diodes showed a photovoltaic performance under AM1.5 illumination, and the conversion efficiency changed depending on the C_{60} evaporation rate.

2. EXPERIMENTAL SECTION

The 500-nm-thick-Cu_2O layer was prepared on a (111)-oriented Au/(100)Si wafer substrate (Kobelco-Kaken) by electrodeposition in an aqueous solution containing 0.2 mol/L copper(II) acetate hydrate and 3 mol/L lactic acid. The solution pH was adjusted to 12.5 by adding a 1 mol/L potassium hydrate aqueous solution. The solution was prepared with reagent grade chemicals and distilled water (15 MΩcm) purified with Millipore Elix Advantage. The electrodeposition was potentiostatically carried out at −0.4 V vs Ag/AgCl reference electrode at 313 K using a potentiostat (HOKUTO−DENKO, HA-501) connected to a coulomb meter (HOKUTO−DENKO, HF-201). The thickness of the Cu_2O layer was controlled by adjusting the electric charge using the coulomb meter. Prior to the deposition, the (111) Au/ (100) Si wafer substrate was polarized at 1 mA cm^2 for 60 s in a 1 mol/L sodium hydroxide aqueous solution and then rinsed with distilled water. The C_{60} layer was prepared on the Cu_2O/(111)-Au/(100) Si wafer and quartz glass substrates by evaporating the C_{60} powder (Frontier Carbon, Co. Ltd., nanom purple TL, 99.9%) using a vacuum evaporation system (ULVAC, VTS 350M/ERH) connected to a vacuum system consisting of a turbo molecular pump and oil-free scroll vacuum pump. The evaporation was carried out under the conditions at ambient temperature and a vacuum of around 3×10^{-4} Pa, and the evaporation rate ranged from 0.25 to 1.0 Å/s using a quartz crystal deposition control system (ULVAC, CRTM-6000G). The hybrid Cu_2O/C_{60} diode was fabricated by stacking 4.7-diphenyl-1.10-phenanthoroline (Bathocuproine; BCP) followed by evaporation of the Al and Ag using the evaporation system.

The thickness was determined by a surface profile measurement system (ULVAC, Dek Tak 150). The X-ray diffraction spectra were recorded by a $\theta-2\theta$ scanning technique with a monochromated CuKα radiation operated at 40 kV and 200 mA using Rigaku RINT 2500 and by a curved imaging plate detector with a monochromated Cu Kα radiation operated at 40 kV and 50 mA using Rigaku RINT-Rapid II. Optical absorption spectra were recorded using a UV−vis−NIR spectrophotometer (Hitachi, U-4100) with a reference to the bare substrate. Electron microscopic observation was carried out with a field-emission scanning electron microscopy (Hitachi, SU8000). The electrical characterization of both Cu_2O and C_{60} layers was carried out by the van-der-Pauw technique using a Hall effect measuring system (Toyo Technica, Resitest 8310) in air at ambient temperature and 0.3T magnetic field. The Cu_2O sample was prepared by mechanically splitting them from the Au/Si substrate followed by fastening in an epoxy resin (Araldite 2091). Four Au ohmic electrodes were prepared on the Cu_2O sample using a vacuum evaporation system (ULVAC, VPC-260F). The 1 μm thick C_{60} layers prepared on the quartz glass substrate were used for the electrical characterization using the Hall effect measuring system. The metallic indium was applied for the electrode due to the work function of 4.1 eV, and four indium electrodes were prepared on the C_{60} sample using the vacuum evaporation system. The electrical characterization was carried out by recording a current density−voltage curve using Keithley 2400 source meter in dark and under AM1.5 illumination with 100 mW cm^{-2} in power.

3. RESULTS AND DISCUSSION

3.1. Structural and Optical Characteristics of C_{60} Layers and the Hybrid Cu_2O/C_{60} Diodes. Figure 1 shows X-ray diffraction patterns recorded for the 500 nm thick C_{60} layers prepared at the evaporation rates of 0.25, 0.50, and 1.0 Å/s on a quartz glass substrate with a curved imaging plate and the 2θ-intensity and β-intensity curves. The radial direction and azimuthal rotation represented the 2θ-angle and β-angle, respectively, as shown in Figure 1a, i. The 2θ intensity curves represented the change in intensity along the 2θ angle at the β angle of 270°, which is the direction normal to the sample surface. One sharp peak and two weak peaks could be observed

dx.doi.org/10.1021/am3006093 | ACS Appl. Mater. Interfaces 2012, 4, 3558−3565

at around 10.7, 17.7, and 20.7° in addition to the broadened peak that originated from the quartz glass substrate on the 2θ intensity curve for the C_{60} layer prepared at the evaporation rate of 0.25 Å/s. It was confirmed for C_{60} layers prepared at the evaporation rate from 0.25 to 1.0 Å/s that three peaks could be observed at 10.74, 17.60, 20.72° on the X-ray diffraction spectra recorded with a conventional $\theta-2\theta$ scanning technique (not shown). The three peaks could be assigned to the (111), (220), and (311) planes of the C_{60} solid with the face-centered cubic (fcc) configuration already reported in the ICDD card.[16] The lattice parameter calculated from the peak angles of the three peaks was 14.19 Å, which was slightly expanded compared to 14.14 Å for a single-crystal C_{60} solid.[17] It was reported that the lattice parameter of the fcc-C_{60} layers prepared by a heteroepitaxial growth technique changed depending on the substrate material and orientation.[18−21] The diffraction angle of the (111) peak showed an almost constant value, regardless of the C_{60} evaporation rate. The intensity of the (111) peak increased with a decrease in the C_{60} evaporation rate, and the maximum intensity was obtained at the evaporation rate of 0.25 Å/s, suggesting a change in the preferred orientation.

The β-intensity curve represented the change in intensity along the β-angle ranging from 180 to 360° at the constant 2θ angle of 10.7°. The intensity changes in a semicircle along the β-angle and shows a maximum at 270 degrees for the randomly oriented sample, such as a powder, because of the absorption effect of the diffracted X-ray radiation by the sample. The intensity for the C_{60} layer prepared at 1.0 Å/s homogeneously dispersed in a semicircle along the β-angle, indicating the random dispersion of the (111) plane. The C_{60} layer prepared at 0.5 Å/s showed semicircle dispersion along the β-angle and weak peak at around 270 degrees. The sharp peak at the β-angle of 270° could be observed for the C_{60} layer prepared at 0.25 Å/s, indicating that the (111) plane of the C_{60} layer with the face-centered cubic configuration was parallel to the surface. The semicircle dispersion remained although the intensity decreased compared to those prepared at 0.50 and 1.0 Å/s. The substrate material and orientation reflected the preferred orientation of the fcc-C_{60} layers in the heteroepitaxial growth, as already reported. The quartz glass substrate does not possess any lattice relationship to the fcc-C_{60} layer, because of the amorphous structure. The existence of the sharp (111) peak and semicircle dispersion suggested that the (111) orientation developed during the layer growth at 0.25 Å/s on the quartz glass substrate, although further investigation is needed.

Figure 2 shows X-ray diffraction patterns recorded with a $\theta-2\theta$ scanning technique for the Au/500-nm-thick-p-Cu_2O/50-nm-thick-C_{60}/BCP/Al diode prepared by stacking the C_{60} layer at 0.25 Å/s. The hybrid Cu_2O/C_{60} diode prepared by stacking the C_{60} layers at the evaporation rate of 0.25 Å/s showed two strong diffracted X-ray peaks identified as the Cu_2O(111) and Au(111) planes and a very weak peak assigned as the C_{60} (111) plane, and the C_{60} (111) peak disappeared at the evaporation rates of 0.50 and 1.0 Å/s on X-ray diffraction spectra recorded by a conventional $\theta-2\theta$ scanning technique, indicating that the tendency of change in the preferred orientation of the C_{60} layer was similar to that on the quartz substrate. Any peak identified as C_{60} solid with the face-centered cubic configuration could not be observed on X-ray diffraction spectra recorded with the curved imaging plate detector.

Figure 3 shows the cross-sectioned structures of the 500 nm thick C_{60} layer prepared on a quartz glass substrate at 0.5 Å/s and the Au/500 nm thick p-Cu_2O/50 nm thick C_{60}/BCP/Al

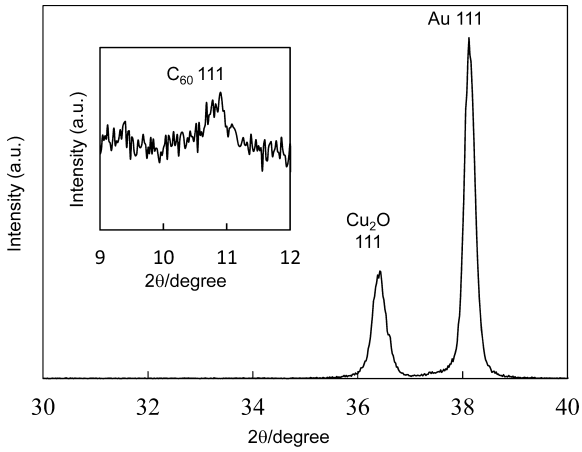

Figure 2. X-ray diffraction spectra for hybrid p-Cu_2O diode with the C_{60} layer prepared at the evaporation rate of 0.25 Å/s.

diode prepared by stacking the C_{60} layer at 0.25 Å/s. The C_{60} layers prepared at 0.25−1.0 Å/s on a quartz glass substrate were composed of columnar grains grown on the substrate and had a very smooth surface. No defects, such as pores, were located throughout the layer thickness and near the interface to the substrate. The grain widths estimated from the surface images were 75.2, 61.1, and 52.8 nm at 0.25, 0.50, and 1.0 Å/s, respectively. The Cu_2O layer was composed of hexagonal columnar grains grown in a direction normal to the substrate surface, which the grain length in the direction vertical to the substrate surface corresponded to the thickness, irrespective of thickness ranging from 250 to 750 nm. The grain width estimated from the image was approximately 110 nm. Any defects, such as pores, could not be located throughout the layer thickness and near the interface to the Au substrate. The Cu_2O layer possessed a (111)-out-of-plane orientation, since there is a lattice relationship of (1 × 1) (111) [$\underline{1}10$] Cu_2O// (1 × 1) (111) [$\underline{1}10$] Au with the lattice mismatch of 4.7% in the a-axis. The electrical characteristic was estimated with a Hall effects measuring system at ambient temperature, and the Cu_2O layer possessed a resistivity of 3.1×10^6 Ω cm with a 9.1×10^{10} cm^{-3} in carrier concentration and 21 $cm^2\ V^{-1}\ s^{-1}$ in mobility.[22]

Figure 4 shows optical absorption spectra for the 500 nm thick C_{60} layers prepared on quartz glass substrate and the hybrid Cu_2O/C_{60} diodes at the C_{60} evaporation rates of 0.25, 0.50, and 1.0 Å/s. Three peaks and a weak shoulder could be observed at the wavelengths of 360, 440, 610, and 510 nm, corresponding to the photon energy of 3.44, 2.81, 2.03, and 2.43 eV, respectively, for C_{60} layers prepared on quartz glass substrate. The absorbance at 610 nm was almost constant for the three C_{60} layers, irrespective of the evaporation rate. The absorbance at 440 nm for the C_{60} layers prepared at 0.25 and 0.50 Å/s was stronger than that at 1.0 Å/s. The absorbance at 360 nm increased with a decrease in the evaporation rate from 1.0 to 0.25 Å/s, and the absorption coefficient calculated from the absorbance and thickness was 5.7×10^4 cm^{-1} for the C_{60} layer prepared at 0.25 Å/s. The absorption spectra for the C_{60} powder dissolved in toluene showed only one absorption peak at around 350 nm, and the absorption at a wavelength ranging from 440 to 620 nm disappeared. It was reported that the absorption bands at a wavelength from 440 to 620 nm were forbidden transitions for isolated molecules, and they become weakly allowed in the solid because of intermolecular

dx.doi.org/10.1021/am3006093 | ACS Appl. Mater. Interfaces 2012, 4, 3558−3565

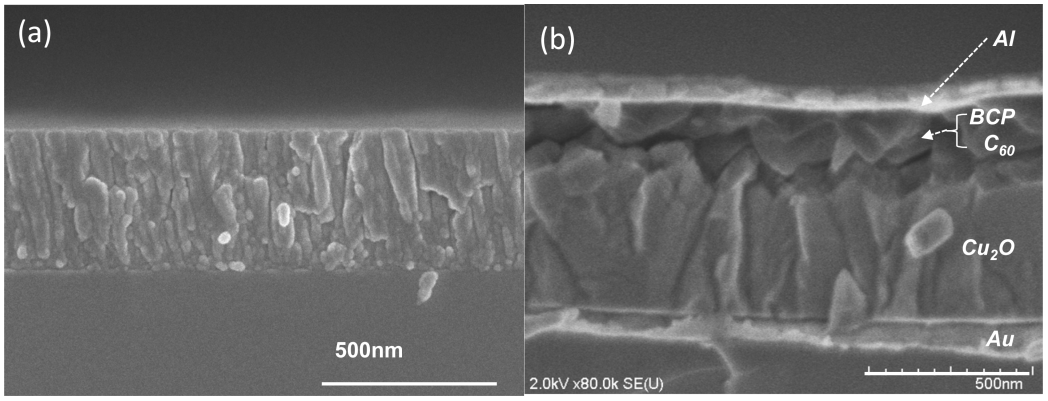

Figure 3. FE-SEM images of cross-sectioned structures of C_{60} layer prepared at evaporation rate of 0.5 A/s on quartz glass substrate and the Au/*p*-Cu_2O/50 nm thick C_{60}/BCP/Al diode.

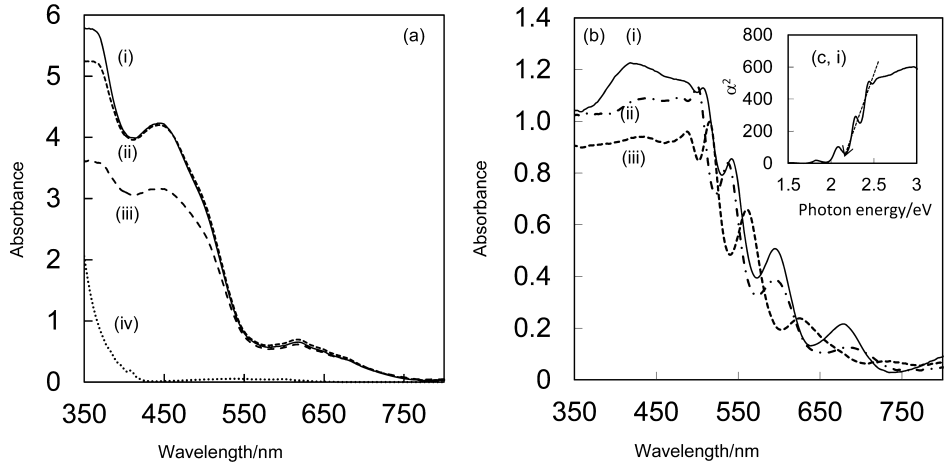

Figure 4. Absorption spectra for (a) C_{60} layers prepared on quartz glass substrate and (b) hybrid Cu_2O/C_{60} diodes at the C_{60} evaporation rate of (i) 0.25, (ii) 0.50, and (iii) 1.0 Å/s and (iv) C_{60} powder dissolved in toluene, and (c, i) the relationship between absorption coefficient (α) and photon energy for the hybrid Cu_2O/C_{60} diode prepared at the C_{60} evaporation rate of 0.25 Å/s.

interactions.[23] This suggested that the configuration of the C_{60} molecules affected the existence and absorbance of the absorption bands at a wavelength ranging from 440 to 620 nm. The absorption bands at around 360 nm were assigned as the electron transition from the ground state to the excited state for generating an exciton inside the C_{60} layer.[10] Because the thickness of the C_{60} layers kept at the constant value of 500 nm, the increase in absorbance at 360 nm suggested that the C_{60} configuration including the preferred orientation affected the electron transition and the amount of generated excitons in the C_{60} layers.

The hybrid Cu_2O/C_{60} diode showed an absorption edge could be observed at wavelength around 650 nm, irrespective of the C_{60} evaporation rate. The fluctuation in absorbance could be observed at wavelength longer than about 500 nm, indicating the homogeneous thickness of the Cu_2O layer. The optical bandgap energy (E_g) was evaluated using the following dependence of the absorption coefficient (α) on the photon energy (E_{pt}): $\alpha^2 \propto (E_{pt} - E_g)$ for the direct transition semiconductor. The bandgap energy was estimated to be 2.1 eV, which was characteristic value for p-Cu_2O semiconductor, irrespective of the C_{60} evaporation rate, as shown in inset. The absorbance at wavelength below 500 nm increased with an increase in the C_{60} evaporation rate. The absorption spectra at wavelength below 500 nm were similar in profile for hybrid Cu_2O/C_{60} diodes prepared at the C_{60} evaporation rate of 0.50 and 1.0 Å/s, and there was a peak with increased absorbance for the hybrid Cu_2O/C_{60} diode prepared at 0.25 Å/s. The absorption coefficient at wavelength of 430 nm was calculated from the absorbance and total thickness of hybrid Cu_2O/C_{60} diode, and the value of 1.6×10^4, 1.8×10^4, and 2.0×10^4 cm^{-1} were obtained for hybrid Cu_2O/C_{60} diodes prepared at the C_{60} evaporation rate of 1.0, 0.50, and 0.25 Å/s, respectively. These values were larger than $1.0 \times 10^4 cm^{-1}$ reported for the (111)-oriented Cu_2O layer prepared on the (111)-Au/Si wafer substrate. Since the absorption coefficient calculated here included those of the C_{60} and Cu_2O layers, the absorption coefficient originated from the C_{60} layer was calculated from the thickness of both layers and absorption coefficient of the Cu_2O semiconductor. The absorption coefficient of the C_{60} layer in the hybrid Cu_2O/C_{60} diode prepared at 0.25 Å/s could be estimated to be approximately 6.0×10^4 cm^{-1}, which was close to $5.7 \times 10^4 cm^{-1}$ estimated for the C_{60} layer prepared on quartz glass substrate at 0.25 Å/s. Because the thickness of the C_{60} layer was kept at a constant value of 50 nm, the increase in absorption coefficient was attributed to the change in the molecular configuration, including preferred orientation of the C_{60} layer as well as those on quartz glass substrate.

The resistivity for C_{60} layers prepared at the C_{60} evaporation rate of 0.25, 0.50, and 1.0 A/s was estimated to be 9×10^8, 1.1

dx.doi.org/10.1021/am3006093 | ACS Appl. Mater. Interfaces 2012, 4, 3558−3565

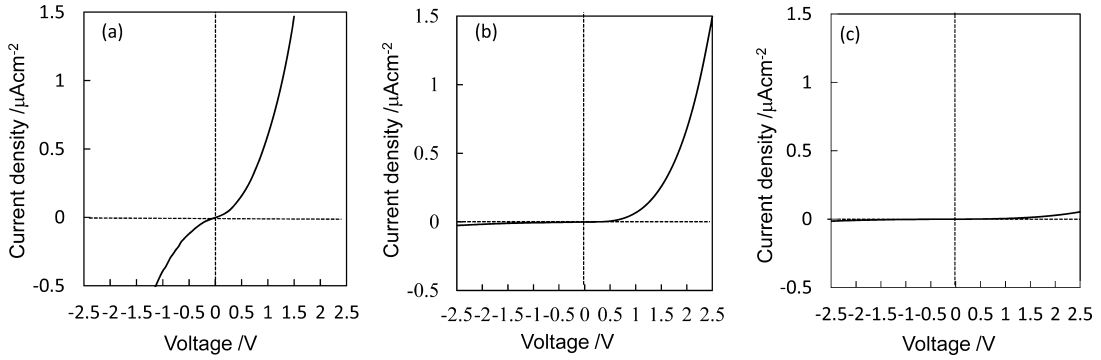

Figure 5. Electrical characteristic for hybrid diode of 50 nm thick C60 and *p*-Cu_2O layer with the thickness of (a) 250, (b) 500, and (c) 750 nm. The C_{60} layer was prepared at evaporation rate of 0.25 Å/s.

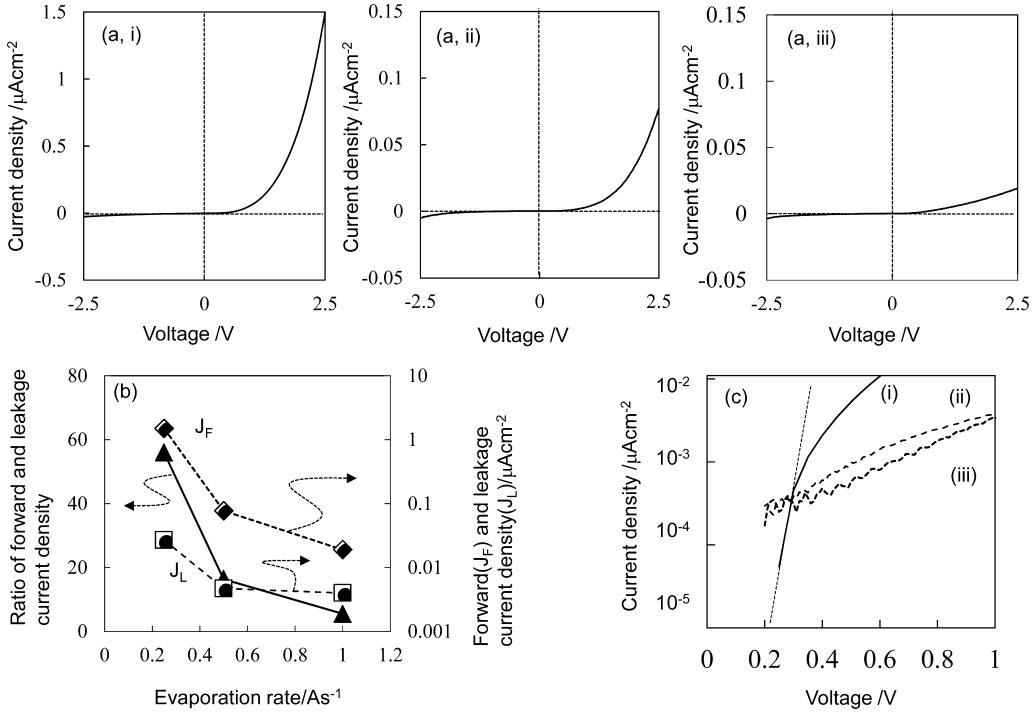

Figure 6. (a) Electrical characteristics for hybrid diodes of 500 nm thick *p*-Cu_2O and 50 nm thick C_{60} layer prepared at evaporation rate of (i) 0.25, (ii) 0.50, and (iii) 1.0 A/s, (b) the dependence of forward and leakage current densities on the evaporation rate, and (c) correlation between the forward current density and forward voltage.

$\times 10^9$, and 1.3×10^9 Ωcm, respectively, but the carrier concentration and mobility could not be estimated because of the high resistivity. Extremely high resistivity of about 4×10^{15} Ω cm was reported for the C_{60} layer prepared by a vacuum sublimation technique,[24] and oxygen involved in air strongly affected to the resistivity in wide range from $\sim 1 \times 10^6$ to 2×10^{10} Ω cm for a single-crystal C_{60} layer.[25] The measurement of the resistivity in this study was carried out in air, and there is a possibility to affect the atmosphere condition to the resistivity. The value at the order of 1×10^9 Ω cm, however, is consistent with the values already reported. The preferred orientation of the C_{60} layer changed from random to ⟨111⟩ and the grain size decreased with decrease in the C_{60} evaporation rate. These results is consistent to the decrease in resistivity, because that the defects in the C_{60} molecular arrangement and grain boundary in the polycrystalline act as the scattering defects for the carrier.

3.2. Electrical Characteristics and Photovoltaic Performance of Hybrid Cu_2O/C_{60} Diode. Figure 5 shows the current density−voltage curves for hybrid diodes of 50-nm thick C_{60} layer prepared at the evaporation rate of 0.25 Å/s and Cu_2O layers with the thickness ranging from 250 to 750 nm. The rectification ratio was estimated by calculating the ratio in current densities at voltages of +1.5 and −1.5 V. The hybrid diode with the 250 nm thick Cu_2O layer showed a poor rectification feature with the rectification ratio of approximately 1.7 and the forward current density of 0.147 μA cm^{-2} at the forward voltage of 1.5 V. The 500 nm thick Cu_2O diode revealed an excellent rectification feature with the rectification ratio of approximately 24 and the forward current density of 1.50 μA cm^{-2} at the forward voltage of 2.5 V. The increase in the Cu_2O thickness to 750 nm induced the deterioration of the rectification ratio to approximately 2.5 and the decrease in the forward current density to 0.077 μA cm^{-2}, which was approximately one twentieth that for the 500 nm thick Cu_2O diode. The Cu_2O layer prepared on the Au(111)/Si wafer substrate showed a (111) preferred orientation because of the small lattice mismatch and possessed high resistivity of 3.1 ×

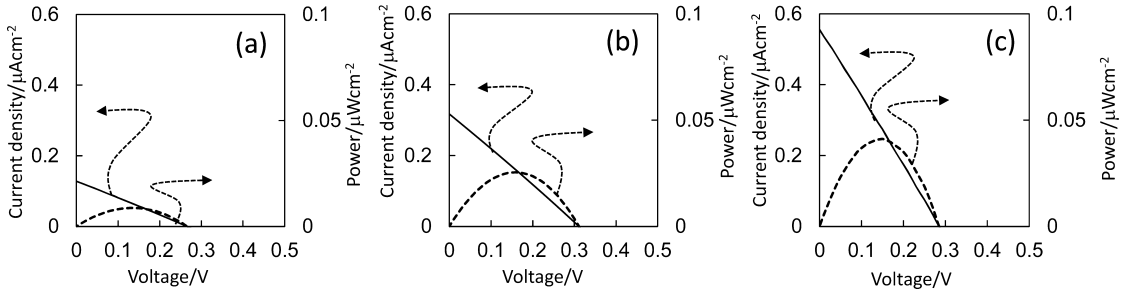

Figure 7. Current density–voltage and power–voltage curves for Ag/C_{60}/Cu_2O/Au photovoltaic devices prepared by stacking the C_{60} layer at the evaporation rate of (a) 0.25, (b) 0.50, and (c) 1.0 Å/s.

10^6 Ω cm, as already reported. The deterioration of the rectification feature with increase in the Cu_2O thickness from 500 to 750 nm is attributed to the high resistivity of the Cu_2O layer. And, the poor rectification with large leakage current density suggested the deterioration of the thickness homogeneity and quality including both the bulk and interface at the Cu_2O thickness of 250 nm, although further investigation is needed.

Figure 6 shows the current density and voltage curves for hybrid Cu_2O diodes of 50 nm thick C_{60} layers prepared at the evaporation rates at 0.25, 0.50, and 1.0 Å/s. The forward (J_F) and leakage current densities (J_L) at +2.5 and −2.5 V and the rectification ratio are summarized in Figure 6b. The hybrid Cu_2O diode of the C_{60} layer prepared at the evaporation rate of 0.25 Å/s showed a 0.027 μA cm^{-2} in leakage current density, 1.50 μA cm^{-2} in forward current density, and the ratio of approximately 57. The increase in the evaporation rate induced a suppression of both the forward and leakage current densities of the hybrid diodes. The forward current density for the C_{60} layers prepared at 0.50 and 1.0 Å/s decreased to 0.077 and 0.019 μA cm^{-2}, respectively, which were about one-twentieth and one-eightieth that at 0.25 Å/s. Also, the leakage current density decreased to −0.0047 and −0.0041 μA cm^{-2}, which were about one-fifth and one-sixth that at 0.25 Å/s. The rectification ratio deteriorated from about 57 to 16.4 and 5.5 at 0.50 and 1.0 Å/s, respectively. It is generally accepted that the relation between the forward current density (J_F) and forward voltage (V_F) is represented by the empirical form as follows[26]

$$J_F \propto \exp(qV_F/\eta KT)$$

where K, q, T, and η are the Boltzmann constant, elementary charge, temperature, and ideality factor, respectively. The relation used for characterizing the p-n junction diodes composed of inorganic semiconductors equals 2 when the recombination current dominates and equals 1 when the diffusion current dominates. Figure 6c shows the plot of the logarithmic value of the forward current density (J_F) versus forward voltage (V_F) for the hybrid Cu_2O diodes prepared at the evaporation rates of 0.25, 0.50, and 1.0 Å/s for the C_{60} layers. The logarithmic value of the forward current density linearly increased with the increase in the forward voltage up to about 0.6 and 1.0 V at the evaporation rates of 0.50 and 1.0 Å/s, respectively. The hybrid Cu_2O diodes prepared at 0.50 and 1.0 Å/s showed large values of 8.9 and 11.1 in ideality factor estimated from the linear part. The hybrid Cu_2O diode prepared by stacking the C_{60} layer at 0.25 Å/s clearly showed the linear part at the forward voltage of less than 0.3 V, and the ideality factor was estimated to be 0.93, which is close to 1 when the diffusion current is dominant for inorganic p-n junction diodes. Since the hybrid Cu_2O diodes were the same in structure and thickness of the Cu_2O and BCP layers, the difference in the electrical characteristic including the change in the ideality factor and the suppression of both the forward and leakage current densities was attributed to the characteristic of the C_{60} layers with the constant thickness of 50 nm.

Figure 7 shows current density–voltage and power–voltage curves recorded for the 500-nm-thick-(111)-Cu_2O/fcc-C_{60}/BCP/Ag diodes prepared by stacking the C_{60} layers at the C_{60} evaporation rate of 0.25, 0.50, 1.0 Å/s under AM1.5 illumination. The conversion efficiency ranging from 8.7 × 10^{-6} to 5.1 × 10^{-5}% was obtained depending on the C_{60} evaporation rate. The open circuit voltage (Voc) showed almost constant value around 0.30 V, and the fill factor (FF) slightly decreased from 0.274 to 0.267 with increase in the C_{60} evaporation rate. The hybrid Cu_2O/C_{60} diodes showed very low short circuit current density (J_{sc}), and the value increased from 0.12 to 0.54 μA cm^{-2} with increase in the C_{60} evaporation rate. The low conversion efficiency was attributed to the very low short-circuit current density.

The photovoltaic performance of 0.20 V in open-circuit voltage (V_{oc}), 67 μA cm^{-2} in short-circuit current density (J_{sc}), 0.25 in fill factor (FF), and 4.2 × 10^{-3}% in conversion efficiency has been reported for the layered hybrid photovoltaic device composed of a randomly oriented Cu_2O electrodeposit and randomly oriented C_{60} layer prepared by a vacuum evaporation technique, but the current density–voltage curves were not shown both in dark and under AM1.5G illumination.[13] The Voc and FF for oriented Cu_2O/C_{60} layered hybrid diodes prepared in this study were improved, but the Jsc was very low compared with those already reported. Clear correlation between the photovoltaic performance and the electrical characteristic such as resistivity of C_{60} layer and rectification feature of the diode could not be observed for (111)-Cu_2O/C_{60}/BCP diodes. It is accepted for organic photovoltaic devices that the short circuit current density closely relates to the diffusion length of excitons generated by light irradiation.[27] The exciton diffusion length was reported to be 400 ± 50 Å for the C_{60} layer prepared by high vacuum evaporation of the C_{60} raw material purified using thermal gradient sublimation[28] and 77 Å for the C_{60} layer prepared by sublimation of a 99%-purity C_{60} material.[29] Because the C_{60} layers embedded in the hybrid diode were prepared by thermal evaporation of industrially employed raw material, the photovoltaic active layer is limited to the vicinity of the heterointeface to the p-Cu_2O layer because of the low exciton diffusion length. The conversion efficiency of the order of 1 × 10^{-5} % and the short circuit current density of the order of 1 × 10^{-4} mA cm^{-2} were close to those already reported for hybrid ZnO/phthalocyanine diodes,[30,31] and the

dx.doi.org/10.1021/am3006093 | ACS Appl. Mater. Interfaces 2012, 4, 3558–3565

exciton diffusion length was reported to be 100 ± 30 Å even for the Cu-phthalocyanine prepared by high vacuum evaporation of purified raw material.[28] Because the thickness of the C_{60} layer used in this study was larger than the diffusion length of excitons generated in the C_{60} layer, the increase in the area of the heterointerface between organic and inorganic semiconductor by introducing a nanomixture structure like the bulk-heterojunction structure embedded in organic photovoltaic devices.

And, the Cu_2O layer act as the light-absorbing layer as demonstrated in the Cu_2O/ZnO photovoltaic device with the conversion efficiency of 1.28% and short-circuit current density (J_{sc}) of 3.8 $mAcm^{-2}$.[7] Although the Ag, BCP, and C_{60} layers were stacked on the Cu_2O layer in the hybrid diode, the intensity of the light irradiated to the under Cu_2O layer was estimated to be about 20% of the light irradiated to the surface of the top Ag layer from the thickness and light-absorbing coefficient of these layers. There is a possibility to loss the carrier generated in the Cu_2O layer at the heterointerface of the C_{60} layer, suggesting the importance of the band-alignment at the heterointerface to transfer the carrier between the Cu_2O and C_{60} layers like the optimum band offset pointed out in compound semiconductor photovoltaic devices such as a $Cu(InGa)Se_2$/CdS/ZnO solar cell.[32]

4. CONCLUSIONS

In this paper, the C_{60} layer with a face-centered cubic configuration was prepared by a vacuum evaporation technique, and the hybrid diode with a 2.1 eV bandgap Cu_2O semiconductor layer was constructed by electrodeposition of the (111)-oriented Cu_2O layer followed by the C_{60} evaporation. The effects of the C_{60} evaporation rate ranging from 0.25 to 1.0 Å/s on the preferred orientation of the C_{60} layer and the rectification feature of the Cu_2O/C_{60} hybrid diode were investigated by structural and electrical characterizations. The preferred orientation of the C_{60} layer with a face-centered cubic configuration changed from random to (111) plane with decrease in the C_{60} evaporation rate from 1.0 to 0.25 Å/s. And, the absorption coefficient that originated from the intermolecular interaction increased at wavelength ranging from 440 to 620 nm. The rectification feature of the Cu_2O/C_{60} hybrid diode strongly depended on the C_{60} evaporation rate, and an excellent rectification feature with the ideality factor of approximately 1 could be obtained for the Au/500 nm thick Cu_2O/50 nm C_{60}/BCP/Al hybrid diode prepared by stacking the C_{60} layer at the evaporation rate of 0.25 Å/s. The 500 nm thick Cu_2O/50 nm thick C_{60} diodes showed a photovoltaic performance ranging from 8.7×10^{-6} to 5.1×10^{-5}% in conversion efficiency with almost constant open circuit voltage (V_{oc}) around 0.30 V, fill factor (FF) around 0.27, and very low short circuit current density (J_{sc}) ranging from 0.12 to 0.54 $\mu A\ cm^{-2}$. Clear correlation could not be observed between the photovoltaic performance and electrical characteristics of Cu_2O, C_{60}, and the rectification feature for the Cu_2O/C_{60}/BCP diodes. The results demonstrated here suggests that importance of the introduction of nanomixture structure like a bulk heterojunction of orgsanic photovoltaic device to collect effectively the carrier generated in the C_{60} layer and the optimization of the energy state at the heterointerfere to transfer the carrier between the Cu_2O and C_{60} layers.

AUTHOR INFORMATION

Corresponding Author

*E-mail: m-izaki@me.tut.ac.jp.

Notes

The authors declare no competing financial interest.

REFERENCES

(1) Vaynzof, Y.; Kabra, D.; Zhao, L.; Ho, P. K. H.; Wee, A. T.-S.; Friend, R. H. *Appl. Phys. Lett.* **2010**, *97*, 033309.
(2) Takanezawa, K.; Tajima, K.; Hashimoto, K. *Appl. Phys. Lett.* **2008**, *93*, 063308.
(3) Beek, W. J. E.; Wienk, M. M.; Kemerink, M.; Yang, X.; Janssen, R. A. J. *J. Phys. Chem.* **2005**, *109*, 9505.
(4) Uchida, S.; Xue, J.; Rand, B. P.; Forrest, S. R. *Appl. Phys. Lett.* **2004**, *84*, 4218.
(5) Suemori, K.; Miyata, T.; Yokoyama, M.; Hiramoto, M. *Appl. Phys. Lett.* **2005**, *86*, 063509.
(6) Mizuno, K.; Izaki, M.; Murase, K.; Shinagawa, T.; Chigane, M.; Inaba, M.; Tasaka, A.; Awakura, Y. *J. Electrochem. Soc.* **2005**, *152*, C179.
(7) Izaki, M.; Shinagawa, T.; Mizuno, K.; Ida, Y.; Inaba, M.; Tasaka, A. *J. Phys. D Appl. Phys* **2007**, *40*, 3326.
(8) Fariza, B. M.; Sasano, J.; Shinagawa, T.; Nakano, H.; Watase, S.; Izaki, M. *J. Electrochem. Soc.* **2011**, *158*, D621.
(9) David, W. I. F.; Ibberson, R. M.; Mattewman, J. C.; Prassides, K.; Dennis, T. J. S.; Hare, J. P.; Kroto, H. W.; Taylor, R.; Walton, D. R. M. *Nature* **1991**, *353*, 147.
(10) Saito, S.; Oshiyama, A. *Phys. Rev. Lett.* **1991**, *66*, 2637.
(11) Xu, H.; Chen, D. M.; Creager, W. N. *Phys. Rev. Lett.* **1993**, *70*, 1850.
(12) Schmicker, D.; Schmidt, S.; Skofronick, J. G.; Toennies, J. P.; Vollmer, R. *Phys. Rev. B* **1991**, *44*, 10995.
(13) Oku, T.; Motoyoshi, R.; Fujimoto, K.; Akiyama, T.; Jeyaderam, B.; Cuya, J. *J. Phys. Chem. Solids* **2011**, *72*, 1206.
(14) Baldo, M. A.; Lamamsky, S.; Burrows, P. E.; Thompson, M. E.; Forrest, S. R. *Appl. Phys. Lett.* **1999**, *75*, 4.
(15) Gommans, H.; Verreet, B.; Rand, B. P.; Muller, R.; Poortmans, J.; Heremans, P.; Genoe, J. *Adav. Funct. Mater* **2008**, *18*, 3638.
(16) Joint Comittttee on Powder Diffraction Standards. *Powder Diffraction File, 44−558*; International Center for Diffraction Data; Swarthmore, PA, 1992
(17) Heiney, P. A.; Fischer, J. E.; McGhie, A. R.; Romanow, W. J.; Denenstein, A. M.; MaCauley, J. P., Jr.; Smith, A. B., III. *Phys. Rev. Lett.* **1991**, *66*, 2911.
(18) Yao, J.; Zou, Y.; Zhang, X.; Chen, G. *Thin Solid Films* **1997**, *305*, 22.
(19) Dura, J. A.; Pippenger, P. M.; Halas, N. J.; Xiong, X. Z.; Chow, P. C.; Moss, S. C. *Appl. Phys. Lett.* **1993**, *63*, 3443.
(20) Zhao, W.; Zhou, W.; Chen, L.; Huang, Y.; Zhang, Z.; Fung, K. K.; Zhao, Z. *J. Solid State Chem.* **1994**, *112*, 412.
(21) Fölsch, S.; Maruno, T.; Yamashita, A.; Hayashi, T. *Appl. Phys. Lett.* **1993**, *62*, 2643.
(22) Izaki, M.; Sasaki, S.; Fariza, BV. M.; Shinagawa, T; Ohta, T.; Watase, S.; Sasano., J. *Thin Solid Films* **2012**, *520*, 1779.
(23) Kazaoui, S.; Ross, R.; Minami, N. *Solid State Commun.* **1994**, *90*, 623.
(24) Mort, J.; Machonkin, M.; Ziolo, R.; Huffman, D. R.; Forguson, M. I. *Appl. Phys. Lett.* **1992**, *60*, 1735.
(25) Arai, T.; Murakami, Y.; Suematsu, H.; Kikuchi, K.; Achiba, Y.; Ikemoto, I. *Solid State Commun.* **1992**, *84*, 827.
(26) Sze, S. M.; Ng, K. K.; *Physics of Semiconductor Devices*, 3rd ed.; Wiley-Interscience: New York, 2007; p 99.
(27) Petterson, L. A. A.; Roman, L. S.; Inganas, O. *J. Appl. Phys.* **1999**, *86*, 487.
(28) Peumans, P.; Yakimov, A.; Forrest, S. R. *J. Appl. Phys.* **2003**, *93*, 3693.
(29) Pettersson, L. A.; Roman, L. S.; Inganas, O *J. Appl. Phys.* **1999**, *86*, 487.

(30) Yoshida, Y.; Nakamura, M.; Tanaka, S.; Hiromitsu, I.; Fujita, Y.; Yoshino, K. *Synth. Met.* **2006**, *156*, 1213.
(31) Stakhira, P. I.; Pakhomov, G. L.; Cherpak, V. V.; Volynyuk, D.; Luka, G.; Godlewski, M.; Guziewicz, E.; Hotra, Z. Y. *Cent. Eur. J. Phys.* **2010**, *8*, 798.
(32) Terada, N.; Widodo, R. T.; Itoh, K.; Kong, S. H.; Kashiwabara, H.; Okuda, T.; Obara, K.; Niki, S.; Sakurai, K.; Yamada, A.; Ishizuka, S. *Thin Solid Films* **2005**, *480−481*, 183.